Toward open-shell nuclei with coupled-cluster theory

G. R. Jansen, M. Hjorth-Jensen, G. Hagen, and T. Papenbrock

Towards open-shell nuclei with coupled-cluster theory

G. R. Jansen,[1] M. Hjorth-Jensen,[1] G. Hagen,[2, 3] and T. Papenbrock[3, 2, 4, 5]

[1]*Department of Physics and Center of Mathematics for Applications, University of Oslo, N-0316 Oslo, Norway*
[2]*Physics Division, Oak Ridge National Laboratory, Oak Ridge, TN 37831, USA*
[3]*Department of Physics and Astronomy, University of Tennessee, Knoxville, TN 37996, USA*
[4]*GSI Helmholtzzentrum für Schwerionenforschung GmbH, 64291 Darmstadt, Germany*
[5]*Institut für Kernphysik, Technische Universität Darmstadt, 64289 Darmstadt, Germany*

We develop a new method based on equation-of-motion coupled-cluster theory to describe properties of open-shell nuclei with $A \pm 2$ nucleons outside a closed shell. We perform proof-of-principle calculations for the ground states of the helium isotopes $^{3-6}$He and the first excited 2^+ state in ^{6}He. The comparison with exact results from matrix diagonalization in small model spaces demonstrates the accuracy of the coupled-cluster methods. Three-particle–one-hole excitations of ^{4}He play an important role for the accurate description of ^{6}He. For the open-shell nucleus ^{6}He, the computational cost of the method is comparable with the coupled-cluster singles-and-doubles approximation while its accuracy is similar to coupled-cluster with singles, doubles and triples excitations.

I. INTRODUCTION

The nuclear shell model is the paradigm for our understanding of atomic nuclei [1]. Within this model, doubly magic nuclei (with fully occupied shells for protons and neutrons) are particularly important because they are stronger bound than their neighbors and can be approximated by a simple product of single-particle states. Within the nuclear shell model, doubly magic nuclei are the cornerstones for our understanding of entire regions of the nuclear chart as they can be viewed as inert cores. For the *ab initio* description of doubly magic nuclei, the coupled cluster (CC) method – based on particle-hole excitations of a reference Slater determinant that obey the linked cluster theorem – is particularly well suited and arguably one of the most efficient methods [2–4]. Similar remarks hold for nuclei that differ from doubly-magic nuclei by one nucleon; such nuclei still exhibit a simple structure and a single Slater determinant is a good reference state. The structure of all other nuclei is more complicated and requires the superposition of many product states and correspondingly large model spaces.

For the light *p*-shell nuclei, various *ab initio* methods [5–11] yield virtually exact results for realistic Hamiltonians. For heavier systems, one typically relies on approximations. Here, coupled-cluster theory is an ideal compromise between accuracy on the one hand and computational cost on the other. This method has been applied to various problems in nuclear structure [2, 3, 12–17].

In this paper, we use equation-of-motion (EOM) techniques within the coupled-cluster method, abbreviated to EOM-CC hereafter, for the description of nuclei that differ from closed-shell references by two nucleons. This extension of the coupled-cluster method is useful for two reasons. First, it significantly enlarges the set of nuclei that can be accessed within coupled-cluster theory. For the oxygen isotopes $^{14-28}$O, for instance, all nuclei except ^{19}O differ from closed-subshell references by two neutrons or less. Similar comments apply to isotopes of helium and calcium. Questions related to the evolution of shell structure [18, 19] could thus be addressed from first principles. Second, the coupled-cluster method yields a similarity transformed Hamiltonian (see Eq. (8) below) for a doubly-magic nucleus. The Hamiltonians for one and two nucleons attached to this doubly magic core provide us with effective single-particle energies and an effective two-body interaction, respectively. These matrix elements could enter the construction of effective shell-model interactions [20] that are the basis for large scale shell-model calculations [21, 22].

Within the EOM-CC methods, the equations for excited states and one particle attached/removed are well known in quantum chemistry [4, 23–27], and have also been applied to atomic nuclei [28–31]. However, the corresponding equations for two particle attached/removed have seen very few applications in quantum chemistry [32, 33] and are new in nuclear physics. In this article, we will thus extend the range of the EOM-CC methods to include open-shell nuclei with $A = \pm 2$ nucleons outside a closed shell core. We present here the necessary formalism for deriving such equations, including the pertinent diagrams and algebraic equations. To our knowledge, these details have not been presented elsewhere. The results from our EOM-CC calculations are compared with full configuration interaction (FCI) calculations for helium isotopes, demonstrating the accuracy of this approach.

This paper is organized as follows. In Sec. II, we give a brief overview of the equation-of-motion method within coupled-cluster theory. The extension of this method to two valence nucleons outside a closed-shell core is presented in Sec. II B. We discuss and present our results in Sec. III. Section IV contains our conclusions and an outlook for future work.

II. COUPLED-CLUSTER THEORY AND EQUATIONS-OF-MOTION FOR NUCLEI

A. Single-reference coupled-cluster theory

In this section we introduce the Hamiltonian that enters our calculation, together with a brief review of single reference coupled-cluster theory. We keep the presentation limited to those details that are required for the derivation of the two particle attached/removed (2PA/PR-EOM-CC) amplitudes presented in Sec. II B. The interested reader is referred to [4] for details.

We use the intrinsic Hamiltonian

$$\hat{H} = \left(1 - \frac{1}{A^*}\right) \sum_{i=1}^{A} \frac{p_i^2}{2m} + \left[\sum_{i<j=1}^{A} \hat{v}_{ij} - \frac{\vec{p}_i \cdot \vec{p}_j}{mA^*}\right] . \quad (1)$$

Here A is the number of nucleons in the reference state, A^* is the mass number of the nucleus that we wish to describe, and $\hat{v}_{ij}$ is the nucleon-nucleon interaction. We will limit ourselves to two-body interactions only. In second quantization, the Hamiltonian can be written as

$$\hat{H} = \sum_{pq} \varepsilon_q^p a_p^\dagger a_q + \frac{1}{4} \sum_{pqrs} \langle pq||rs\rangle a_p^\dagger a_q^\dagger a_s a_r . \quad (2)$$

The term $\langle pq||rs\rangle$ is a shorthand for the matrix elements (integrals) of the two-body part of the Hamiltonian of Eq. (1), p, q, r and s represent various single-particle states while ε_q^p stands for the matrix elements of the one-body operator in Eq. (1). Finally, operators like $a_q^\dagger$ and a_p create and annihilate a nucleon in the state q and p, respectively. These operators fulfill the canonical anti-commutation relations.

In single-reference coupled-cluster theory, the many-body ground-state $|\Psi_0\rangle$ is given by the exponential ansatz,

$$|\Psi_0\rangle = \exp\left(\hat{T}\right)|\Phi_0\rangle . \quad (3)$$

Here, $|\Phi_0\rangle$ is a single-reference Slater determinant, and $\hat{T}$ is the cluster operator that generates correlations. The operator $\hat{T}$ is expanded as a linear combination of particle-hole excitation operators

$$\hat{T} = \hat{T}_1 + \hat{T}_2 + \ldots + \hat{T}_A \quad (4)$$

where $\hat{T}_n$ is the n-particle-n-hole excitation operator

$$\hat{T}_n = \left(\frac{1}{n!}\right)^2 \sum_{a_\nu i_\nu} t_{i_1\ldots i_n}^{a_1\ldots a_n} a_{a_1}^\dagger \ldots a_{a_n}^\dagger a_{i_n} \ldots a_{i_1} . \quad (5)$$

We use throughout this work the convention that the indices $ijk\ldots$ denote states below the Fermi level (holes), while the indices $abc\ldots$ denote states above the Fermi level (particles). For an unspecified state, the indices $pqr\ldots$ are used. The amplitudes $t_{i_1\ldots i_n}^{a_1\ldots a_n}$ will be determined by solving the coupled-cluster equations. In the

singles and doubles approximation we truncate the cluster operator as

$$\hat{T} \approx \hat{T}_{\text{CCSD}} \equiv \hat{T}_1 + \hat{T}_2 , \quad (6)$$

which defines the coupled-cluster approach with singles and doubles excitations, the so-called CCSD approximation. The unknown amplitudes result from the solution of the CCSD equations given by

$$\begin{aligned} \langle \Phi_i^a | \bar{H} | \Phi_0 \rangle &= 0, \\ \langle \Phi_{ij}^{ab} | \bar{H} | \Phi_0 \rangle &= 0 . \end{aligned} \quad (7)$$

The term

$$\bar{H} = \exp\left(-\hat{T}\right)\hat{H}\exp\left(\hat{T}\right) = \left(\hat{H}\exp\left(\hat{T}\right)\right)_C , \quad (8)$$

is the similarity transform of the normal-ordered Hamiltonian. The state $|\Phi_{ij\ldots}^{ab\ldots}\rangle$ is a Slater determinant that differs from the reference $|\Phi_0\rangle$ by holes in the orbitals $ij\ldots$ and by particles in the orbitals $ab\ldots$. The subscript C indicates that only connected diagrams enter.

Once the t_i^a and t_{ij}^{ab} amplitudes have been determined from Eq. (7), the correlated ground-state energy is given by

$$E_{\text{CC}} = \langle \Phi_0 | \bar{H} | \Phi_0 \rangle + E_0 . \quad (9)$$

Here, E_0 denotes the vacuum expectation value with respect to the reference state. The coupled-cluster equations (7) show that the reference state $|\Phi_0\rangle$ is an eigenstate of the similarity transformed Hamiltonian (8) within the space of 1p-1h and 2p-2h excitations.

B. Equation-of-motion coupled-cluster theory for nuclei with $A \pm 2$ nucleons outside a closed shell.

In this work, our focus is on the development of coupled-cluster theory for nuclei that differs from a closed shell by two nucleons. These are systems where no single reference can be constructed without breaking symmetries (such as rotational invariance). One could apply the CCSD method to the deformed (symmetry breaking) Hartree-Fock ground state of an open-shell nucleus. However, the restoration of angular momentum requires more than singles and doubles cluster excitations (see for example Ref. [15]) and is computationally expensive. Here, we wish to stay within the computationally inexpensive CCSD scheme.

Open-shell systems can be computed with multi-reference methods. In such an approach, many reference wave functions are included and treated on an equal footing. However, the loss of mathematical simplicity and transparency, and problems related to intruder states make these multi-reference approaches difficult to pursue. For a detailed discussion, we refer the reader to Ref. [34]. Equation-of-motion methods (see [26, 27] for recent reviews) avoid these problems as they exhibit the transparency and computational simplicity of single-reference coupled-cluster theory.

Within the EOM-CCSD approach, the states of the $A \pm 2$ open-shell nuclei are computed from the ground state of the A-body system as

$$|\Psi_\mu^{(A\pm2)}\rangle = \hat{R}_\mu^{(A\pm2)}|\Psi_0^{(A)}\rangle = \hat{R}_\mu^{(A\pm2)}\exp{(\hat{T})}|\Phi_0\rangle . \quad (10)$$

Here, $\hat{R}_\mu^{(A\pm2)}$ is a particle removal or particle addition operator that generates an $(A \pm 2)$-body state from the A-body coupled-cluster wave function. The label μ identifies the quantum numbers (energy, angular momentum, ...) of the state of interest.

The operator $\hat{R}_\mu$, and the energies E_μ of the states of interest solve the eigenvalue problem [4, 23–27]

$$(\bar{H}\hat{R}_\mu^{(A\pm2)})_C|\Phi_0\rangle = \omega_\mu \hat{R}_\mu^{(A\pm2)}|\Phi_0\rangle . \quad (11)$$

Here, the expression $(\bar{H}\hat{R}_\mu^{(A\pm2)})_C$ denotes all terms that connect the similarity transformed Hamiltonian $\bar{H}$ with the excitation operator $R_\mu^{(A\pm2)}$. The energy difference $\omega_\mu \equiv E_\mu - E_0^*$ is the excitation energy of the state μ in the nucleus $A \pm 2$ with respect to the ground state energy E_0^* of the closed shell reference nucleus with the "mass shift" $A* = A \pm 2$. This mass shift in the intrinsic Hamiltonian (1) ensures that the correct kinetic energy of the center-of- mass is utilized in computing the $A \pm 2$ nuclei.

The operators $\hat{R}_\mu$ relevant for this work are (we drop the label μ for convenience)

$$\hat{R}^{(A+2)} = \frac{1}{2}\sum_{ba} r^{ab} a_a^\dagger a_b^\dagger + \frac{1}{6}\sum_{iabc} r_i^{abc} a_a^\dagger a_b^\dagger a_c^\dagger a_i + \dots (12)$$

$$\hat{R}^{(A-2)} = \frac{1}{2}\sum_{ij} r_{ij} a_i a_j + \frac{1}{6}\sum_{ijka} r_{ijk}^a a_a^\dagger a_k a_j a_i + \dots , (13)$$

where the unknown amplitudes r (subscripts and superscripts dropped) can be grouped into a vector that solves the eigenvalue problem of Eq. (11). The operator (12) consists of a $2p$-$0h$ term, a $3p$-$1h$ term, and in general up to an $(A + 2)p$-Ah term. In this work, we will truncate the operator (12) at the $3p$-$1h$ level. Clearly, this truncation will only be a good approximation for states in the $(A \pm 2)$-body system that have a relatively simple structure built on the A-body nucleus. We will introduce two different truncations for the particle attached and the particle removed method, and identify them by the number of particle-hole excitations kept in the operator (12). A truncation after the first term in Eq. (12) is referred to as 2PA-EOM-CCSD($2p$-$0h$), while the truncation after the second term is denoted as 2PA-EOM-CCSD($3p$-$1h$). Similarly for 2PR-EOM-CCSD, we will use the abbreviations 2PR-EOM-CCSD($0p$-$2h$) and 2PR-EOM-CCSD($1p$-$3h$) for truncations after the first and second term in Eq. (13), respectively. Table I shows the excitation operators used in these truncation schemes.

We construct the matrix (i.e., the connected part of $\bar{H}\hat{R}$) of the eigenvalue problem of Eq. (11) diagrammatically. As usual, lines directed upwards represent particle states, while lines directed downwards represent hole

Operator	Expression
$\hat{R}_{2p-0h}^{A+2}$	$\frac{1}{2}\sum_{ab} r^{ab} a_a^\dagger a_b^\dagger$
$\hat{R}_{3p-1h}^{A+2}$	$\frac{1}{2}\sum_{ab} r^{ab} a_a^\dagger a_b^\dagger + \frac{1}{6}\sum_{abci} r_i^{abc} a_a^\dagger a_b^\dagger a_c^\dagger a_i$
$\hat{R}_{0p-2h}^{A-2}$	$\frac{1}{2}\sum_{ij} r_{ij} a_j a_i$
$\hat{R}_{1p-3h}^{A-2}$	$\frac{1}{2}\sum_{ij} r_{ij} a_j a_i + \frac{1}{6}\sum_{aijk} r_{ijk}^a a_a^\dagger a_k a_j a_i$

Table I: Definition of the EOM excitation operators for the two particles attached (removed) method, using a truncation at both the 2-particle-0-hole (0-particle-2-hole) and 3-particle-1-hole (1-particle-3-hole) level. The operator $\hat{R}_{2p-0h}^{A+2}$ defines 2PA-EOM-CCSD($2p$-$0h$), the operator $\hat{R}_{3p-1h}^{A+2}$ defines 2PA-EOM-CCSD($3p$-$1h$), the operator $\hat{R}_{0p-2h}^{A-2}$ defines 2PR-EOM-CCSD($0p$-$2h$) while the operator $\hat{R}_{1p-3h}^{A-2}$ defines 2PR-EOM-CCSD($1p$-$3h$). These operators enter the eigenvalue problem of Eq. (11).

Amplitude	Diagram
r^{ab}	
r_{ij}	
r_i^{abc}	
r_{ijk}^a	

Table II: Diagrams corresponding to the excitation operators defined in Table I. Upward directed lines denote unoccupied orbitals (particle states) and downward directed lines denote occupied orbitals (hole states). The heavy horizontal line represents the operator vertex, used to distinguish the $\hat{R}$ operators from the similarity transformed Hamiltonian $\bar{H}$.

states [4]. The horizontal lines represent the operators and we use a heavy and a wiggly line too differentiate the two operators in the composite diagrams. Table II shows the diagrams corresponding to the r amplitudes, while the matrix elements of the similarity-transformed Hamiltonian are represented by the diagrams shown in Table III. These elements are well known and computed from the corresponding contractions of the cluster operator (6) with the Hamiltonian of Eq. (1) (see, for instance, Ref. [4]). They result from the construction of the operator (8) after the CCSD equations (7) have been solved.

Table IV shows the algebraic expressions for the matrix elements of the similarity-transformed Hamiltonian $\bar{H}$. For notational efficiency, some intermediate objects (χ) that are common among several of the matrix elements, are defined separately in Table V. In the numer-

Matrix element	Diagram
$\langle i|\bar{H}|a\rangle$	
$\langle a|\bar{H}|b\rangle$	
$\langle i|\bar{H}|j\rangle$	
$\langle ai|\bar{H}|bc\rangle$	
$\langle ij|\bar{H}|ka\rangle$	
$\langle ab|\bar{H}|cd\rangle$	
$\langle ij|\bar{H}|kl\rangle$	
$\langle ia|\bar{H}|bj\rangle$	
$\langle ab|\bar{H}|ci\rangle$	
$\langle ia|\bar{H}|jk\rangle$	
$\langle abc|\bar{H}|dei\rangle$	
$\langle ija|\bar{H}|klm\rangle$	
$\langle aib|\bar{H}|cdj\rangle$	
$\langle ija|\bar{H}|kbl\rangle$	

Table III: Diagrams of the matrix elements of the similarity-transformed Hamiltonian $\bar{H}$. The horizontal wiggly line represents the operator vertex. The top three diagrams represent the one-body matrix elements of $\bar{H}$, the last four diagrams represent the three-body matrix elements of $\bar{H}$, and the remaining diagrams denote two-body matrix elements of $\bar{H}$, respectively. The corresponding algebraic expressions are shown in Table IV.

ical implementation, the storage of the similarity transformed Hamiltonian requires some memory. However, this modest cost in memory yields a significant reduction in computational cycles. For a detailed analysis we refer the reader to Refs. [35, 36].

In a diagrammatic language, the left-hand-side of the

Matrix element	Shorthand	Expression
$\langle i|\bar{H}|a\rangle$	$\bar{H}_a^i$	$f_a^i + \langle im||ae\rangle t_m^e$
$\langle a|\bar{H}|b\rangle$	$\bar{H}_b^a$	$\chi_b^a - \frac{1}{2}\langle mn||be\rangle t_{mn}^{ae}$
		$-t_m^a \bar{H}_b^m$
$\langle i|\bar{H}|j\rangle$	$\bar{H}_j^i$	$f_j^i + \langle im||je\rangle t_m^e$
		$+\frac{1}{2}\langle im||ef\rangle t_{jm}^{ef} + t_j^e \bar{H}_e^i$
$\langle ai|\bar{H}|bc\rangle$	$\bar{H}_{bc}^{ai}$	$\chi_{bc}^{ai} - \frac{1}{2}\langle mi||bc\rangle t_m^a$
$\langle ij|\bar{H}|ka\rangle$	$\bar{H}_{ka}^{ij}$	$\chi_{ka}^{ij} + \frac{1}{2}\langle ij||ea\rangle t_k^e$
$\langle ab|\bar{H}|cd\rangle$	$\bar{H}_{cd}^{ab}$	$\langle ab||cd\rangle + \frac{1}{2}\langle mn||cd\rangle t_{mn}^{ab}$
		$-\hat{P}(ab)t_m^b \chi_{cd}^{am}$
$\langle ij|\bar{H}|kl\rangle$	$\bar{H}_{kl}^{ij}$	$\langle ij||kl\rangle + \frac{1}{2}\langle ij||ef\rangle t_{kl}^{ef}$
		$+\hat{P}(kl)t_l^e \chi_{ke}^{ij}$
$\langle ia|\bar{H}|bj\rangle$	$\bar{H}_{bj}^{ia}$	$\chi_{bj}^{ia} + \frac{1}{2}\langle mi||eb\rangle t_{jm}^{ae}$
$\langle ab|\bar{H}|ci\rangle$	$\bar{H}_{ci}^{ab}$	$\frac{1}{2}\langle ab||ce\rangle t_i^e + \chi_{ci}^{ab} - t_{mi}^{ab}\bar{H}_c^m$
		$-\frac{1}{2}t_{mn}^{ab}\bar{H}_{ic}^{mn} + \hat{P}(ab)t_{mi}^{eb}\bar{H}_{ce}^{am}$
		$-\hat{P}(ab)t_m^a {\chi'}_{ci}^{mb}$
$\langle ia|\bar{H}|jk\rangle$	$\bar{H}_{jk}^{ia}$	$\chi_{jk}^{ia} + t_{jk}^{ea}\bar{H}_e^i$
		$+\hat{P}(jk)t_{mk}^{ea}\bar{H}_{je}^{im} - \frac{1}{2}t_m^a \bar{H}_{jk}^{im}$
$\langle abc|\bar{H}|dei\rangle$	$\bar{H}_{dei}^{abc}$	$\hat{P}(a,bc)\langle mn||de\rangle t_m^a t_{ni}^{bc}$
		$-\hat{P}(a,bc)\langle am||de\rangle t_{mi}^{bc}$
$\langle ija|\bar{H}|klm\rangle$	$\bar{H}_{klm}^{ija}$	$\hat{P}(k,lm)\langle ij||ke\rangle t_{lm}^{ea}$
		$+\hat{P}(k,lm)\langle ij||ef\rangle t_k^e t_{lm}^{fa}$
$\langle aib|\bar{H}|cdj\rangle$	$\bar{H}_{cdj}^{aib}$	$-\langle mi||cd\rangle t_{mj}^{ab}$
$\langle ija|\bar{H}|kbl\rangle$	$\bar{H}_{kbl}^{ija}$	$\langle ij||eb\rangle t_{kl}^{ea}$

Table IV: Algebraic expressions for the matrix elements of the similarity-transformed Hamiltonian in terms of the cluster amplitudes t_i^a and t_{ij}^{ab}, the matrix elements $\langle ij||ef\rangle$ of the two-body interaction, and the one-body matrix elements $f_q^p = \varepsilon_q^p + \sum_i \langle pi|v|qi\rangle$ of the normal-ordered Hamiltonian. The permutation operator $\hat{P}_{pq}$ permutes the indices p and q, and we define $\hat{P}(pq) = 1 - \hat{P}_{pq}$, $\hat{P}(pq,r) = 1 - \hat{P}_{pr} - \hat{P}_{qr}$, and $\hat{P}(p,qr) = 1 - \hat{P}_{pq} - \hat{P}_{pr}$. The intermediates χ are defined in Table V.

Intermediate	Expression
χ_b^a	$f_b^a + \langle am||be\rangle t_m^e$
χ_{bc}^{ai}	$\langle ai||bc\rangle - \frac{1}{2}\langle mi||bc\rangle t_m^a$
χ_{ka}^{ij}	$\langle ij||ka\rangle + \frac{1}{2}\langle ij||ea\rangle t_k^e$
${\chi''}_{bj}^{ia}$	$\langle ia||bj\rangle + \frac{1}{2}\langle ai||eb\rangle t_j^e$
${\chi'}_{bj}^{ia}$	${\chi''}_{bj}^{ia} + \frac{1}{2}\langle ai||eb\rangle t_j^e - \frac{1}{2}t_m^a \bar{H}_{jb}^{mi}$
χ_{bj}^{ia}	${\chi'}_{bj}^{ia} - \frac{1}{2}t_m^a \bar{H}_{jb}^{mi} + \frac{1}{2}\langle mi||eb\rangle t_{jm}^{ae}$
χ_{ci}^{ab}	$\langle ab||ci\rangle + \frac{1}{2}\langle ab||ce\rangle t_i^e$
χ_{jk}^{ia}	$\langle ia||jk\rangle + \frac{1}{2}\langle ia||ef\rangle t_{jk}^{ef} + P(jk)t_j^e {\chi''}_{ek}^{ia} - \frac{1}{2}t_m^a \bar{H}_{jk}^{im}$

Table V: The intermediates that enter the construction of the similarity-transformed Hamiltonian $\bar{H}$ in Table IV. All other terms are defined in Table IV.

eigenvalue problem (11) consists of all topologically different diagrams that result from connecting a diagram from Table II with a diagram in Table III. Figures 1 and 2 show the diagrams of $(\bar{H}\hat{R})_C$ for the two truncations of the 2PA-EOM-CCSD method. Let us briefly discuss some of these diagrams.

For 2PA-EOM-CCSD(2p-0h), the relevant diagrams correspond to the matrix element $\langle \Phi^{ab}|(\bar{H}\hat{R})_C|\Phi_0\rangle$, i.e., they have two outgoing particle lines and consist of con-
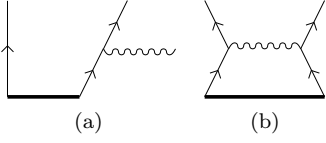
Figure 1: Diagrams corresponding to the matrix element $\langle\Phi^{ab}|(\bar{H}\hat{R})_C|\Phi_0\rangle$ for the 2PA-EOM-CCSD(2p-0h) amplitude equation. All diagrams are constructed by contracting a diagram from Table II, with a diagram from Table III. Only diagrams that satisfy the topological form of $\langle\Phi^{ab}|(\bar{H}\hat{R})_C|\Phi_0\rangle$, with two external particle lines in the upper part of the diagram and no external lines in the bottom part of the diagram, are selected.
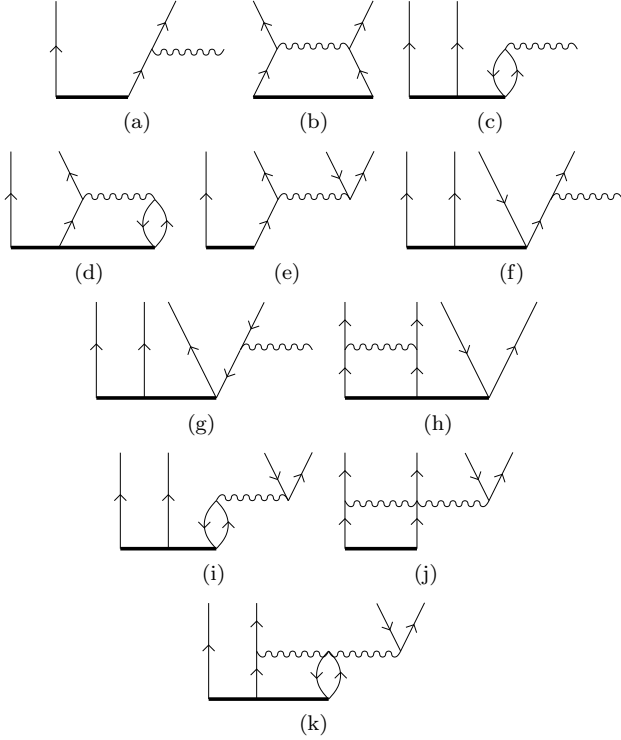

Figure 2: Diagrams corresponding to the matrix elements $\langle\Phi^{ab}|(\bar{H}\hat{R})_C|\Phi_0\rangle$ (a-d) and $\langle\Phi^{abc}_i|(\bar{H}\hat{R})_C|\Phi_0\rangle$ (e-k) for the 2PA-EOM-CCSD(3p-1h) amplitude equation.

Figure 3: Diagrams corresponding to the matrix element $\langle\Phi_{ij}|(\bar{H}\hat{R})_C|\Phi_0\rangle$ for the 2PR-EOM-CCSD(0p-2h) amplitude equation. All diagrams are constructed by contracting a diagram from Table II, with a diagram from Table III. Only diagrams that satisfy the topological form of $\langle\Phi_{ij}|(\bar{H}\hat{R})_C|\Phi_0\rangle$, with two external hole lines in the upper part of the diagram and no external lines in the bottom part of the diagram, are selected.

Figure 4: Diagrams corresponding to the matrix elements $\langle\Phi_{ij}|(\bar{H}\hat{R})_C|\Phi_0\rangle$ (a-d) and $\langle\Phi^a_{ijk}|(\bar{H}\hat{R})_C|\Phi_0\rangle$ (e-k) for the 2PR-EOM-CCSD(1p-3h) amplitude equation.

tractions of the similarity transformed Hamiltonians with r^{ab}. As an example, consider the diagram of Fig. 1(b). It results from contracting the diagram of r^{ab} (cf. Table II), with the diagram of $\langle ab|\bar{H}|cd\rangle$ (cf. Table III). For 2PA-EOM-CCSD(3p-1h) additional diagrams of the form $\langle\Phi^{ab}|(\bar{H}\hat{R})_C|\Phi_0\rangle$ enter because the amplitude r^{abc}_i is also permitted. In addition, diagrams corresponding to the matrix element $\langle\Phi^{abc}_i|(\bar{H}\hat{R})_C|\Phi_0\rangle$ (i.e., diagrams with three outgoing particle lines and one incoming hole line) enter. The diagram in Fig. 2(h), for instance, is constructed by contracting the diagram element representing r^{abc}_i in Table II, with the diagram element representing $\langle ab|\bar{H}|cd\rangle$ in Table III.
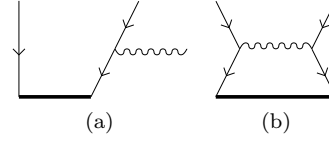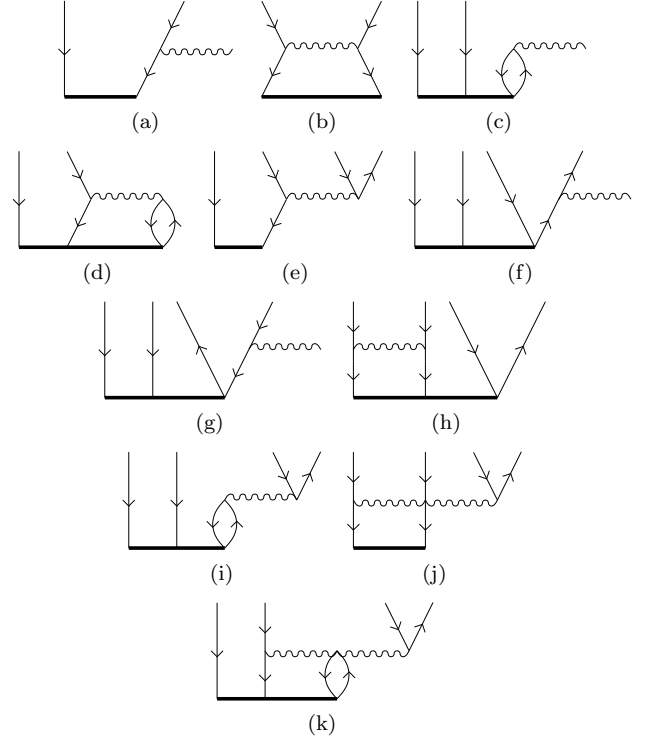
Let us turn to the diagrams for two-particle removal.

Figures 3 and 4 show the diagrams of $(\bar{H}\hat{R})_C$ for the two truncations of the 2PR-EOM-CCSD method. Here, one needs topologies of the form $\langle\Phi_{ij}|(\bar{H}\hat{R})_C|\Phi_0\rangle$ and $\langle\Phi^a_{ijk}|(\bar{H}\hat{R})_C|\Phi_0\rangle$ using the r_{ij} and r^a_{ijk} diagrams in Table II.

The algebraic expressions corresponding to these diagrams are derived according to the standard rules, see for example Ref. [4], and shown in Table VI. The computational cost is $n^5_u n_o$ for the 2PA-EOM-CCSD(3p-1h) method, and the most expensive diagram is shown in Fig. 2(h). Likewise, the most expensive diagram for the 2PR-EOM-CCSD(1p-3h) is shown in Fig. 4(i) and requires of the order of $n^2_u n^4_o$ operations. Here, n_u is the number of unoccupied orbitals (equal to the size of the va-

Matrix element	Expression
2PA-EOM-CCSD($2p$-$0h$):	
$\langle\Phi^{ab}\|(\bar{H}\hat{R})_C\|\Phi_0\rangle$	$\hat{P}(ab)\bar{H}^b_e r^{ae} + \frac{1}{2}\bar{H}^{ab}_{ef} r^{ef}$
2PA-EOM-CCSD($3p$-$1h$):	
$\langle\Phi^{ab}\|(\bar{H}\hat{R})_C\|\Phi_0\rangle$	$\hat{P}(ab)\bar{H}^b_e r^{ae} + \frac{1}{2}\bar{H}^{ab}_{ef} r^{ef}$
	$+\bar{H}^m_e r^{abe}_m + \frac{1}{2}\hat{P}(ab)\bar{H}^{bm}_{ef} r^{aef}_m$
$\langle\Phi^{abc}_i\|(\bar{H}\hat{R})_C\|\Phi_0\rangle$	$\hat{P}(a,bc)\bar{H}^{bc}_{ei} r^{ae} + \hat{P}(ab,c)\bar{H}^c_e r^{abe}_i$
	$-\bar{H}^m_i r^{abc}_m + \frac{1}{2}\hat{P}(ab,c)\bar{H}^{ab}_{ef} r^{efc}_i$
	$+\hat{P}(ab,c)\bar{H}^{mc}_{ei} r^{abe}_m + \frac{1}{2}\bar{H}^{abc}_{efi} r^{ef}$
	$+\frac{1}{2}\hat{P}(a,bc)\bar{H}^{bmc}_{efi} r^{aef}_m$
2PR-EOM-CCSD($0p$-$2h$):	
$\langle\Phi_{ij}\|(\bar{H}\hat{R})_C\|\Phi_0\rangle$	$-\hat{P}(ij)\bar{H}^m_j r_{im} + \frac{1}{2}\bar{H}^{mn}_{ij} r_{mn}$
2PR-EOM-CCSD($1p$-$3h$):	
$\langle\Phi_{ij}\|(\bar{H}\hat{R})_C\|\Phi_0\rangle$	$-\hat{P}(ij)\bar{H}^m_j r_{im} + \frac{1}{2}\bar{H}^{mn}_{ij} r_{mn}$
	$+\bar{H}1^m_e r^e_{ijm} - \frac{1}{2}\hat{P}(ij)\bar{H}^{mn}_{je} r^e_{imn}$
$\langle\Phi^a_{ijk}\|(\bar{H}\hat{R})_C\|\Phi_0\rangle$	$-\hat{P}(i,jk)\bar{H}^{ma}_{jk} r_{im} + \bar{H}^a_e r^e_{ijk}$
	$-\hat{P}(ij,k)\bar{H}^m_k r^a_{ijm} + \frac{1}{2}\hat{P}(ij,k)\bar{H}^{mn}_{ij} r^a_{mnk}$
	$+\hat{P}(ij,k)\bar{H}^{ma}_{ek} r^e_{ijm} + \frac{1}{2}\bar{H}^{mna}_{ijk} r_{mn}$
	$-\frac{1}{2}\hat{P}(i,jk)\bar{H}^{mna}_{jek} r^e_{imn}$

Table VI: Algebraic expressions for the 2PA/2PR-EOM-CCSD($2p$-$0h$/$0p$-$2h$) and 2PA/2PR-EOM-CCSD($3p$-$1h$/$1p$-$3h$) approximations. All terms are defined in Table IV.

lence space), and n_o is the number of occupied orbitals in the reference state. For comparison, the computational costs of the single-reference CCSD and CCSDT methods are $n^4_u n^2_o$ and $n^5_u n^3_o$, respectively. This shows that the 2PA/2PR-EOM-CC methods developed in this work are relatively inexpensive from a computational point of view, and comparable to the cost of CCSD. Note that the three-body matrix elements of the similarity-transformed Hamiltonian are not stored. Instead, they are calculated when needed and do not contribute significantly to the overall cost of the calculations. For a detailed analysis we refer the reader to Refs. [35, 36].

The eigenvalue problem of Eq. (11) for the two-particle attached system thus becomes

$$\langle\Phi^{ab}|(\bar{H}\hat{R})_C|\Phi_0\rangle = \omega r^{ab}$$
$$\langle\Phi^{abc}_i|(\bar{H}\hat{R})_C|\Phi_0\rangle = \omega r^{abc}_i \ . \quad (14)$$

Here, the left-hand-side is a linear function of the "vector" $R = (r^{ab}, r^{abc}_i)$ of amplitudes (see Table VI) and constitutes a matrix-vector product. Note that the two equations are coupled and constitute a single eigenvalue problem for the $3p$-$1h$ truncation. Likewise, we find for the two-particle removed problem

$$\langle\Phi_{ij}|(\bar{H}\hat{R})_C|\Phi_0\rangle = \omega r_{ij}$$
$$\langle\Phi^a_{ijk}|(\bar{H}\hat{R})_C|\Phi_0\rangle = \omega r^a_{ijk} \ . \quad (15)$$

We are usually only interested in the few lowest eigenvalues of Eq. (11). For this purpose, we use the Arnoldi Method for asymmetric eigenvalue problems, see for example Ref. [37] and references therein. This method is based on repeated applications of the matrix-vector product $(\bar{H}\hat{R})_C$. Specifically, our numerical implementation uses the ARPACK software [38] package. The expressions in Table VI can thus be used to solve the eigenvalue problem directly. In this paper, we employ the m-scheme basis for the vectors $R = (r^{ab}, r^{abc}_i)$ of the 2PA. Within this scheme, we are limited to small model spaces. However, in this work we are mainly interested in testing the newly developed methods and in gauging the accuracy of the employed cluster truncation through comparisons with exact diagonalization. Note that the similarity-transformed Hamiltonian $\bar{H}$ exhibits the symmetries of the underlying Hamiltonian. In the m-scheme basis, we can classify states by their projections J_z of angular momentum and T_z of isospin and their parity. Although the solutions will have a good total angular momentum $\hat{J}^2$, we will not be able to exploit this symmetry in the m-scheme basis.

The FCI method we employ [39] is limited to relatively small model spaces. Note, however, that we are also working on an angular-momentum-coupled implementation [40] of 2PA/2PR-EOM-CCM. This will allow us to exploit rotational symmetries and give us access to much larger model spaces. These spaces are well beyond the reach of present full diagonalization methods.

III. RESULTS

For the proof-of-principle study we consider the helium isotopes ^{3}He to ^{6}He. Here, ^{3}He and ^{5}He are viewed as one neutron removed from and attached to ^{4}He, respectively. In a shell-model picture, ^{6}He is a truly open-shell nucleus with two valence neutrons in the $p_{3/2}$ shell. Thus, a single-reference Slater determinant may not be a good starting point for coupled-cluster calculations of this nucleus, and it seems advantageous to describe this six-nucleon system as two (halo) neutrons added to the ^{4}He core. We do not present results for ^{2}He using the 2PR-EOM-CCSD approach; an analysis of this method will be presented elsewhere [40].

For our calculations we use a realistic nucleon-nucleon (NN) potential derived from chiral effective field theory [41–45] at order N^{3}LO using interaction matrix elements from Ref. [45]. The matrix elements of the bare interaction employ a cutoff at $\Lambda = 500$ MeV. The short-range parts of the interaction are removed via the similarity renormalization group transformation [46] with a cutoff at 1.9 fm^{-1}. We use the spherical harmonic oscillator with the oscillator frequency $\hbar\omega = 24$ MeV as our single-particle basis. Our model space consists of five major oscillator shells, with maximum orbital angular momentum $l_{\max} = 2$. This results in a total of 76 single-particle states for neutrons and protons. We neglect three-body

and four-body interactions. This leads to missing many-body physics but is not relevant for our proof-of-principle computation and comparison with FCI calcualtions.

We calculate the ground state energies of the A= 3-6 helium isotopes. For ^{6}He we also compute the first 2^+ state and the expectation values of the total angular momentum. In addition, we also discuss the first 1^- excited state, as an example where the $3p$-$1h$ truncation fails. We compare the equation-of-motion (EOM) approach to the FCI method and to three different single-reference coupled-cluster approximations. Recall that within the m-scheme, one can also compute open-shell nuclei directly with the coupled-cluster method without resorting to EOM techniques. While such a direct approach may suffer from the lack of a good reference state (as is the case for the ground state of ^{6}He), the inclusion of more and more clusters must converge to the FCI results. Comparing the EOM-CC approach to these single-reference coupled-cluster calculations allows us to gauge the efficiency of the various coupled-cluster approximations.

The direct coupled-cluster calculations employ the CCSD approximation described above, the CCSDT approximation (that includes triples clusters) and the CCSDT-1 approach which includes some of the $3p$-$3h$ clusters of the full CCSDT approximation. For the EOM calculations, we use the CCSD wave function of ^{4}He as the reference wave function and employ the intrinsic Hamiltonian of Eq. (1) with $A = 3, 5, 6$ for ^{3,5,6}He, respectively. We compare all results to an exact calculation done with the FCI approach, using the same interaction and model space. The ground-state energies of $^{3-5}$He are shown in Table VII. For ^{3}He, CCSDT becomes an exact method and agrees with FCI. Here, the single-reference coupled-cluster calculations are superior to the EOM-CCSD approach. Evidently, the weakly bound nucleus ^{3}He is not well described as a neutron removed from the tightly bound ^{4}He. This means in turn that correlations beyond one-particle-two-hole excitations play a non-negligible role. For ^{4}He, the EOM-CCSD approach is identical to CCSD. Here, triples corrections and full triples represent a significant improvement over CCSD, bringing the results close to the FCI ones. For ^{5}He, the EOM-CCSD is superior to a single-reference CCSD calculation and competes well with the computationally more expensive triples correction CCSDT-1. Clearly, the valence neutron in ^{5}He is weakly correlated with the strongly bound ^{4}He core, and the PA-EOM-CCSD approach captures this state very well.

We turn to the open-shell nucleus ^{6}He and show our results in Table VIII. Here, the 2PA-EOM-CCSD ($3p$-$1h$) approach is clearly superior to the single-reference coupled-cluster approaches, as it reproduces the energy and the spin of the ground state to a very good approximation. For the computation of the spin within the single-reference approaches, we compute the expectation value $\langle J^2 \rangle$ within the Hellmann-Feynman theorem, and define $\langle J \rangle$ from the relation $\langle J^2 \rangle = \langle J \rangle (\langle J \rangle + 1)$. A direct

	^{3}He	^{4}He	^{5}He
CCSD	−6.624	−27.468	−22.997
CCSDT-1	−6.829	−27.600	−23.381
CCSDT	−6.911	−27.619	−23.474
EOM-CCSD	−6.357	−27.468	−23.382
FCI	−6.911	−27.640	−23.640

Table VII: Ground-state energies (in MeV) for ^{3}He, ^{4}He and ^{5}He, calculated with coupled-cluster methods truncated at the 2-particle-2-hole (CCSD) level, 3-particle-3-hole (CCSDT) and a hybrid (CCSDT-1) where a small subset of the leading diagrams in CCSDT are included. For the EOM-CCSD approach, truncations has been made at the 1-particle-2-hole level, the 2-particle-2-hole level, and the 2-particle-1-hole level for ^{3}He, ^{4}He and ^{5}He respectively. The energies are compared to the exact full configuration interaction (FCI).

	0^+_1	2^+_1	$0^+ \langle J \rangle$	$2^+_1 \langle J \rangle$
CCSD	−22.732	−20.905	0.78	2
CCSDT-1	−24.617	−21.586	0.25	2
CCSDT	−24.530	−21.786	0.01	2
2PA-EOM-CCSD($2p$-$0h$)	−21.185	−18.996	0	2
2PA-EOM-CCSD($3p$-$1h$)	−24.543	−21.634	0	2
FCI	−24.853	−21.994	0	2

Table VIII: Energies (in MeV) for the ground state and first excited state of ^{6}He and the expectation value of the total angular momentum, calculated with coupled-cluster methods truncated at the 2-particle-2-hole (CCSD) level, 3-particle-3-hole (CCSDT) and a hybrid (CCSDT-1) where the 3-particle-3-hole amplitudes are treated perturbatively. The 2PA-EOM-CCSD results are calculated with a truncation at the 2-particle-0-hole (2PA-EOM-CCSD($2p$-$0h$)) level and at the 3-particle-1-hole (2PA-EOM-CCSD($3p$-$1h$)) level. All energies are compared to full configuration interaction (FCI) results.

computation within the CCSD or CCSDT approximations can only be based on a symmetry-breaking reference state. Clearly, 2-particle-2-hole excitations (CCSD) cannot restore the symmetry, and we find that $\langle J \rangle = 0.78$ for the ground state of ^{6}He. Adding 3-particle-3-hole excitations (CCSDT approximation) almost restores the rotational symmetry, but some correlation energy is still missing. In the 2PA-EOM-CCSD approach, however, the rotational symmetry is preserved throughout the calculation, and we obtain a very good approximation of the energy at a relatively low computational cost. As expected, the 2PA-EOM-CCSD ($2p$-$0h$) approach is less accurate than the $3p$-$1h$ approximation, since it is unable to account simultaneously for the correlations within the three-body system consisting of the two valence neutrons and the ^{4}He core. The ground state and the first excited 2^+ state of ^{6}He are both dominated by a configuration with two neutrons in the $p_{3/2}$ orbit. This is consistent with the shell-model picture of this nucleus. For the excited 2^+_1 state, the CCSD, CCSDT and CCSDT-1 methods result in the correct value of the angular momentum due to the choice of reference state.

Let us define the fraction σ_{corr} of the correlation energy as

$$\sigma_{\text{corr}} = \frac{E_{2\text{PA}} - E_0}{E_{\text{FCI}} - E_0} \ . \tag{16}$$

Here $E_{2\text{PA}}$ is the energy from 2PA-EOM-CCSD, E_{FCI} is the energy from the FCI, while E_0 is the energy expectation of the uncorrelated reference state $|\Phi_0\rangle$. Both E_{2PA} and E_{FCI} are shown in Table VIII, and $E_0 = -16.807$ MeV. We also compute the norm

$$\mathcal{N} = \sum_{ab} |r^{ab}|^2 + \sum_{abi} |r_i^{ab}|^2 \ . \tag{17}$$

The normalized squared weights

$$\rho_1^2 \equiv \mathcal{N}^{-1} \sum_{ab} |r^{ab}|^2$$
$$\rho_2^2 \equiv \mathcal{N}^{-1} \sum_{abi} |r_i^{ab}|^2 \ , \tag{18}$$

fulfill $\rho_1^2 + \rho_2^2 = 1$ and measure the importance of the $2p$-$0h$ and $3p$-$1h$ amplitudes, respectively.

Table IX shows the relative correlation energies σ_{corr} and the relative weights ρ_1 and ρ_2 of 2PA-EOM-CCSD($3p$-$1h$) for the three lowest states with quantum numbers 0^+, 1^- and 2^+ of ^{6}He, respectively. We see that 2PA-EOM-CCSD accounts for more than 90% of the correlation energy for the 0^+ and 2^+ states, and that most of the weight is carried by the $2p$-$0h$ amplitude. The 1^- state, however, is not very accurately reproduced and much of the correlation energy is lacking. For this state, the 2PA-EOM-CCSD($3p$-$1h$) energy is $E_{1^-} = -20.95$ MeV and deviates considerably from the full CI result $E_{1^-} = -23.26$ MeV. Consistent with this picture is the large weight carried by the $3p$-$1h$ amplitudes. For a converged computation, one would presumably also need to include $4p$-$2h$ or higher clusters. Inspection shows that the $J^\pi = 1^-$ state is dominated by two neutrons in the $0p_{3/2}$ single-particle state, but with an additional 1-particle–1-hole excitation of either a proton or a neutron to the $0p_{3/2}$ state or the $0p_{1/2}$ orbit. These $3p$-$1h$ configurations are energetically favored compared with a configuration with one neutron in the $0p_{3/2}$ state and one in the $0d_{5/2}$ state, a configuration which can also give a 1^- state. This explains why this state is dominated by the r_i^{abc} amplitudes. Note finally that we cannot expect a separation of the center-of-mass motion from the intrinsic dynamics in the small model space we considered [31, 47]. Such a separation, if it exists, must be investigated further in larger model spaces. Thus, the low-lying 1^- state might also exhibit considerable admixtures with spurious center-of-mass excitation.

We have shown that EOM works very well for nuclei with two valence nucleons that are dominated by two-particle excitations on top of a correlated core. Moreover, the EOM wave function preserves the symmetries of the Hamiltonian and is expected to be useful in the computation of matrix elements besides the energy. Taking

	σ_{corr}	ρ_1	ρ_2
0_1^+	0.96	0.84	0.16
1_1^-	0.64	0.34	0.66
2_1^+	0.93	0.81	0.19

Table IX: The relative correlation energy σ_{corr} defined in Eq. (16) for the lowest states with quantum numbers $J^\pi = 0^+$, 1^- and 2^+ in ^{6}He, respectively. The relative weights ρ_1 and ρ_2 of the $2p$-$0h$ and $3p$-$1h$ amplitudes, respectively, are defined in Eqs. (18).

into account the low computational cost of the EOM-CC methods as compared to the full CCSDT approach, our EOM approach is clearly well suited for these selected states. For states where more complicated particle-hole excitations are prominent, the various truncation schemes discussed here are insufficient and we will need additional correlations in the EOM operator to reach satisfactory results. The ground state of ^{3}He and the first excited 1^- state of ^{6}He discussed above, are examples in case.

IV. CONCLUSIONS AND FUTURE PERSPECTIVES.

We have developed and implemented the equation-of-motion coupled-cluster method and performed microscopic calculations of helium isotopes with up to two valence nucleons outside the closed-shell alpha particle. The comparison with full configuration interaction calculations shows that the equation-of-motion coupled-cluster methods yield accurate results for sufficiently simple states. The open-shell nucleus ^{6}He, for instance, can be viewed and computed as two weakly correlated neutrons attached to the correlated core of ^{4}He. The proof-of-principle calculations were performed in a reduced model space for a comparison with results from exact diagonalizations. We are working on implementing our formalism for the two-particle attached and removed equation-of-motion coupled-cluster methods in an angular momentum coupled basis. This will allow us to employ much larger model spaces. With this improvement, the first-principles computation of semi-magic nuclei, single-particle energies, and effective two-particle interactions for the nuclear shell-model can be addressed.

[1] M. G. Mayer and J. H. D. Jensen, in *Nobel Lectures in Physics 1963-1970* (Elsevier, Amsterdam, 1972).
[2] F. Coester and H. Kümmel, Nucl. Phys. **17**, 477 (1960).
[3] H. Kümmel, K. H. Lührmann, and J. G. Zabolitzky, Phys. Rep. **36**, 1 (1978).
[4] I. Shavitt and R. J. Bartlett, *Many-body methods in Chemistry and Physics*, (Cambridge, 2009).
[5] H. Kamada, *et al.*, Phys. Rev. C **64**, 044001 (2001).
[6] K. Varga and Y. Suzuki, Phys. Rev. C **52**, 2885 (1995).
[7] N. Barnea, W. Leidemann, and G. Orlandini, Phys. Rev. C **61**, 054001 (2000).
[8] R. B. Wiringa and S. C. Pieper, Annu. Rev. Nucl. Part. Sci. **51**, 53 (2001).
[9] P. Navrátil, S. Quaglioni, I. Stetcu, and B. R. Barrett, J. Phys. G **36**, 083101 (2009).
[10] E. Epelbaum, H. Krebs, D. Lee, and U.-G. Meissner, Phys. Rev. Lett. **104**, 142501 (2010).
[11] E. Epelbaum, H. Krebs, D. Lee, and U.-G. Meissner, Eur. Phys. J. A **45**, 335 (2010).
[12] R. F. Bishop, M. F. Flynn, M. C. Boscá, E. Buendiá, and R. Guardiola, Phys. Rev. C **42**, 1341 (1990).
[13] J. H. Heisenberg and B. Mihaila, Phys. Rev. C **59**, 1440 (1999).
[14] D. J. Dean and M. Hjorth-Jensen, Phys. Rev. C **69**, 054320 (2004).
[15] G. Hagen, D. J. Dean, M. Hjorth-Jensen, and T. Papenbrock, Phys. Lett. B **656**, 169 (2007).
[16] M. Horoi, J. R. Gour, M. Włoch, M. D. Lodriguito, B. A. Brown, and P. Piecuch, Phys. Rev. Lett. **98**, 112501 (2007).
[17] G. Hagen, T. Papenbrock, D. J. Dean, and M. Hjorth-Jensen, Phys. Rev. Lett. **101**, 092502 (2008).
[18] O. Sorlin and M. G. Porquet, Prog. Part. Nucl. Phys. **61**, 602 (2008).
[19] R. Kanungo *et al*, Phys. Rev. Lett. **102**, 152501 (2009).
[20] M. Hjorth-Jensen, T. T. S. Kuo, and E. Osnes, Phys. Rep. **261**, 125 (1995).
[21] B. A. Brown, Prog. Part. Nucl. Phys. **47**, 517 (2001).
[22] M. Honma, T. Otsuka, B. A. Brown, and T. Mizusaki, Phys. Rev. C **69**, 034335 (2004).
[23] M. Nooijen and J. G. Snijders, Int. J. Quantum Chem. **48**, 15 (1993).
[24] M. Nooijen and R. J. Bartlett, J. Chem. Phys. **102**, 3629 (1995).
[25] J. F. Stanton and J. Gauss, J. Chem. Phys. **103**, 1064 (1995).
[26] A. I. Krylov, Annu. Rev. Phys. Chem. **59**, 433 (2008)
[27] P. Piecuch, J. R. Gour, and M. Włoch, Int. J. Quantum Chem. **109**, 3268 (2009).
[28] M. Włoch, D. J. Dean, J. R. Gour, M. Hjorth-Jensen, K. Kowalski, T. Papenbrock, and P. Piecuch, Phys. Rev. Lett. **94**, 212501 (2005).
[29] J. R. Gour, P. Piecuch, M. Hjorth-Jensen, M. Włoch, and D. J. Dean, Phys. Rev. C **74**, 024310 (2006).
[30] G. Hagen, T. Papenbrock, and M. Hjorth-Jensen, Phys. Rev. Lett. **104**, 182501 (2010).
[31] G. Hagen, T. Papenbrock, D. J. Dean, and M. Hjorth-Jensen, Phys. Rev. C **82**, 034330 (2010).
[32] M. Nooijen and R. J. Bartlett, J. Chem. Phys. **107**, 6812 (1997).
[33] M. Wladyslawski and M. Nooijen, Adv. Quant. Chem. **49**, 1 (2005).
[34] R. J. Bartlett, Int. J. Mol. Sci., **3**, 579 (2002).
[35] S. A. Kucharski and R. J. Bartlett, Adv. Quantum Chem. **18**, 281 (1986).
[36] G. Hagen, T. Papenbrock, D. J. Dean, A. Schwenk, A. Nogga, M. Włoch, and P. Piecuch, Phys. Rev. C **76**, 034302 (2007).
[37] G. H. Golub and C. F. Van Loan, *Matrix Computations*, (Johns Hopkins University Press, Baltimore, 1996).
[38] R. B. Lehoucq, D. C. Sorensen, and Y. Yang, *ARPACK User's Guide: Solution to large scale eigenvalue problems with implicitly restarted Arnoldi methods*, SIAM Publications, Philadelphia (1998); FORTRAN code available under http://www.caam.rice.edu/software/ARPACK/.
[39] T. Papenbrock and D. J. Dean, Phys. Rev. C **67**, 051303 (2003); T. Papenbrock, A. Juodagalvis, and D. J. Dean Phys. Rev. C **69**, 024312 (2004).
[40] G. R. Jansen *et al.*, in preparation.
[41] S. Weinberg, Physics Letters B **251**, 288 (1990).
[42] S. Weinberg, Nuclear Physics B **363**, 3 (1991).
[43] P. Bedaque and U. van Kolck, Annu. Rev. Nucl. Part. Sci. **52**, 339 (2002).
[44] E. Epelbaum, H.-W. Hammer, and U.-G. Meißner, Rev. Mod. Phys. **81**, 1773 (2009).
[45] D. R. Entem and R. Machleidt, Phys. Rev. C **68**, 041001 (2003).
[46] S. K. Bogner, R. J. Furnstahl, and R. J. Perry, Phys. Rev. C **75**, 061001 (2007).
[47] G. Hagen, T. Papenbrock, and D. J. Dean, Phys. Rev. Lett. **103**, 062503 (2009).